Darwin theory of heterostructure diffraction

S. M. Durbin and G. C. Follis

Department of Physics, Purdue University, West Lafayette, Indiana 47907

A simplified approach to calculating the two-beam x-ray reflectivity of any planar heterostructure crystal is presented. Darwin's recursion formulas are applied to the individual atomic planes of any layered structure, and the reflectivity is calculated numerically. The results are exact for arbitrary composition profiles and essentially all angles, without requiring crystalline periodicity. This method is equally useful for perfect crystal substrates with submonolayer surface layers, for superlattices, or for arbitrary multilayer structures.

I. INTRODUCTION

X-ray reflectivity measurements are important for the characterization of heterostructures grown by molecular beam epitaxy (MBE) and other fabrication techniques which control the composition of individual atomic layers. Because the substrates are usually wafers of GaAs, Si, or other nearly perfect material, dynamical diffraction theory must be used to describe the substrate reflectivity. A kinematic description may be adequate for the overlayer if its reflectivity is sufficiently low, permitting a hybrid calculation of the total reflectivity combining the dynamical substrate with the kinematic overlayer. If the overlayer is strongly reflecting, however, the entire crystal must be treated dynamically. While dynamical theory is exactly solvable for undistorted perfect crystals, the situation for strained or composite crystals is generally more complicated. In this paper we present a computational method based on Darwin's dynamical diffraction theory, which is both exact and based on an intuitive picture of building up the heterostructure out of individual atomic planes.

We will compare this Darwin recursion method with two standard approaches, the Takagi-Taupin extension of the standard von Laue dynamical diffraction theory[1,2] and the Abelès optical model as applied to x rays by Berreman and Macrander.[3-5] The general problem can be described as determining the relation between microscopic structure and macroscopic optical phenomena when the wavelengths are of atomic dimensions.

Von Laue showed that the short-wavelength x-ray response of a perfect crystal could be described by writing a microscopic dielectric "constant" which is proportional to the local electron density.[6] After incorporating Ewald's concepts of the reciprocal lattice and the dispersion surfaces, von Laue reduced the problem to applying Fresnel boundary conditions to the solutions of Maxwell's equations with this microscopically varying dielectric constant. Both Takagi and Taupin extended the von Laue theory to a strained crystal, by assigning to each region a local reciprocal lattice and matching the solutions from one region to the next. More recently the Takagi-Taupin differential equations have been reformulated as recursion relations,[7,8] which are better suited for calculating reflectivities of arbitrary heterostructures.

While von Laue's theory represents the atomic structure of a crystal by a triply periodic dielectric constant, the Abelès optical theory replaces the crystal by lamellae of uniform dielectric constant.[3,5] The distance between adjacent atomic planes is divided into N sublayers, with each sublayer assigned a uniform dielectric constant proportional to the local average electron density, in the same manner as in the von Laue theory. The propagation of electromagnetic radiation from one layer to the next is determined by solving Maxwell's equations with a dielectric constant which is a function of the distance from an interface. These solutions, which yield the Fresnel boundary conditions in the limit of a single abrupt interface, can be expressed in terms of a characteristic matrix for each of the lamellae.

Because this is a direct space calculation, with no reciprocal lattice, the Abelès approach is well suited for reflectivities of arbitrary, nonperiodic multilayer structures. It is similar to Parratt's earlier method for calculating the reflectivity of x-ray mirrors by modeling the physical surface as N stratified, homogeneous media.[9] Parratt's optical approach was in fact utilized in some of the earliest analyses of x-ray reflectivity from semiconductor superlattices.[10] Berreman and co-workers have since demonstrated that the Abelès matrix method reproduces the Laue perfect crystal results, and the results of Takagi-Taupin calculations for various heterostructures.

The Darwin method we employ has no dielectric constants, no Fresnel boundary conditions, and no reciprocal lattice.[11] As the first theory of dynamical diffraction, it is based on the individual atomic electrons being driven into forced oscillations, generating spherical waves which propagate at the speed of light in vacuum. The amplitudes reflected and transmitted by a single atomic plane of infinite lateral extent are calculated, and the Darwin recursion relations are derived for a crystal made up of a periodic array of such planes. As we show below, these recursion relations can equally well be applied to a nonperiodic arrangement of planes.

This Bragg geometry derivation is similar in spirit to Howie and Whelan's application of Darwin theory to the Laue transmission geometry in thin, distorted crystals.[12] The similarity in the forms of the Takagi-Taupin equa-

<u>51</u>   10 127

tions and the Darwin recursion relations has been previously noted,[13] and, further, the Darwin results have been derived with the Abelès characteristic matrix method,[14] both natural consequences of the common electromagnetic theory which underpins all dynamical theories. What distinguishes the present work, however, is that the amplitude from each atomic plane in the structure is explicitly calculated, a feat made possible only by the continued rapid improvements in computer power. The main advantage of this approach is that the calculation has the same "structure" as the physical structure fabricated by the crystal grower, because in both cases the focus is on the order and composition of individual atomic layers.

II. DERIVATION OF THE HETEROSTRUCTURE X-RAY REFLECTIVITY

In the following sections, we review Darwin's theory for a semi-infinite perfect crystal, extend it to the presence of a single surface layer added to the perfect crystal, and then generalize the recursion relations to an arbitrary number and type of overlayers.

A. Semi-infinite perfect crystal

We first summarize Darwin's results for the x-ray reflectivity of a perfect semi-infinite crystal, which is modeled as a regular stack of perfect planes of infinite lateral extent. These planes consist of scatterers arranged in a periodic array in empty space. By summing the spherical electromagnetic waves caused by the forced oscillations of all the scatterers, Darwin showed that at a distant point a specular wave is observed with reflectivity

$$R = -ir_e\lambda MF(2\theta)/\sin\theta$$
$$\equiv -iq, \tag{1}$$

where $r_e = e^2/mc^2$ is the classical electron radius, λ is the wavelength, $F(2\theta)$ is the structure factor of the scatterer, and θ is the angle of incidence. (For simplicity we consider only perpendicular polarization.) Several approximations have been made here. First, the monolayer is of infinite lateral extent. This is an excellent approximation to a finite layer if the lateral dimensions are somewhat larger than the first Fresnel zone diameter,

$$L = \frac{2}{\sin\theta}\left(\frac{\lambda r}{2}\right)^{\frac{1}{2}}, \tag{2}$$

where r is the distance from the specimen to the detector, which must be much larger than interatomic separations.[15] Second, the waves emitted by the scatterers have a negligible influence on other parts of that same monolayer. That is, only the incident wave determines the forced oscillations of the scatterers. This requires that the singularity at $\theta = 0$ be avoided, which in practice excludes grazing angles below a few milliradians, or somewhat less than typical critical angles for total reflection (from semi-infinite solids). Third, we will shortly

assume that this plane wave describes the wave field inside the crystal itself, not just at a distant detector. This is generally valid because only a negligible fraction of the wave field seen by a given plane will originate from the immediately adjoining layers, from which the spherical waves emitted by the discrete scatterers are not yet fully superposed into plane waves.

The same type of summation which produces the specular plane wave yields a forward scattered plane wave, which must be added to the incident beam to form the total transmitted beam. Its amplitude is denoted by $-iq_o$, which is the same as in Eq. (1) except that the forward scattering structure factor $F(0)$ is used instead of $F(2\theta)$. Hence there are three beams associated with a single monolayer, the incident, transmitted, and reflected waves. When we consider a stack of many monolayers, however, the transmitted beam from one layer becomes the incident beam on the next, so all waves are accounted for by assigning an incident and scattered wave to each plane. Letting T_r and S_r denote the amplitudes of the incident and scattered waves evaluated at the rth plane, Darwin derived the following recursion relations for adjacent planes:

$$S_r = -iq_rT_r + (1 - iq_{o,r})e^{i\phi_r}S_{r+1},$$
$$T_{r+1} = (1 - iq_{o,r})e^{i\phi_r}T_r - iq_re^{i2\phi_r}S_{r+1}, \tag{3}$$

where $\phi_r = 2\pi d(\sin\theta)/\lambda$ and d is the separation between the r and $r + 1$ planes. The scattering geometry is illustrated in Fig. 1. The first equation gives two components for the wave reflected by the rth layer: the fraction of the incident beam directly reflected $(-iq_r)$, as well as the wave reflected by the $r + 1$ plane underneath, corrected for its phase advance $(e^{i\phi_r})$ and for transmission through the rth plane, $(1 - iq_{o,r})$. Because the reflectivity per plane is low, the higher-order reflections proportional to q^3, q^5, etc., are ignored. The second equation similarly gives the transmitted components only to order q.

To simplify the discussion, we rewrite these recursion relations as

$$S_r = \alpha_rT_r + \beta_rS_{r+1},$$
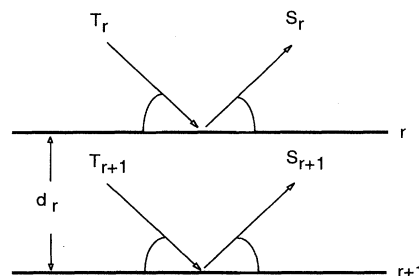$$T_{r+1} = \gamma_rT_r + \delta_rS_{r+1}. \tag{4}$$

FIG. 1. The Darwin scattering geometry. The transmitted (T_r) and scattered (S_r) field amplitudes denote their values at the rth plane, and d_r is the distance to the next plane.

Since every plane in the semi-infinite crystal is identical, Darwin observed that the change in amplitude at each plane must be independent of the plane, so

$$T_{r+1} = x T_r. \tag{5}$$

Inserting this into the recursion relations leads to the solution

$$S_0/T_0 \equiv R_0 = \frac{\alpha}{1 - \beta x}, \tag{6}$$

where the subscripts have been dropped from α and β because each plane is identical. S_0 and T_0 refer to the topmost plane of the crystal, so their ratio is the total reflectivity. The complex constant x is the solution of the quadratic equation

$$\beta x^2 + (\alpha \delta - \beta \gamma - 1)x + \gamma = 0. \tag{7}$$

Equations (6) and (7) can be simplified in the neighborhood of a Bragg reflection to produce analytical expressions yielding the famous "Darwin curve," but with computers it is much simpler to numerically determine the exact solution, always choosing the root of the quadratic equation which decreases the wave intensity with increasing depth into the crystal.

B. Adding a surface monolayer

We now consider how the reflectivity of the homogeneous semi-infinite crystal is modified by a single surface monolayer. As the topmost plane of the perfect crystal was indexed $r = 0$, this overlayer will be denoted by -1. We can simply write down Eqs. (3) or (4) with $r = -1$ and $r + 1 = 0$. The inputs q_{-1} and $q_{o,-1}$ depend only on the scatterers in the overlayer, and ϕ_{-1} contains the height of the overlayer. By substituting Eq. (6) into the recursion relations, we obtain

$$S_{-1} = \alpha_{-1} T_{-1} + \beta_{-1} R_0 T_0,$$
$$T_0 = \gamma_{-1} T_{-1} + \delta_{-1} R_0 T_0. \tag{8}$$

These further reduce to

$$\frac{S_{-1}}{T_{-1}} \equiv R_{-1} = \alpha_{-1} + \frac{\beta_{-1} \gamma_{-1} R_0}{1 - \delta_{-1} R_0}. \tag{9}$$

R_{-1} is the reflectivity of the total system comprising the perfect semi-infinite substrate and the overlayer. Equation (9) is an exact expression for the so-called "truncation-rod" scattering of a monolayer on a dynamically diffracting substrate, valid even at the Bragg peaks where kinematic expressions are not. Note that it was not necessary to solve a quadratic equation, once the substrate reflectivity R_0 was known.

C. Multilayer structures

By repeating the above analysis for a second and further monolayers, one finds immediately that Eq. (9) can be generalized to relate the reflectivities at any pair of successive planes:

$$R_r = \alpha_r + \frac{\beta_r \gamma_r R_{r+1}}{1 - \delta_r R_{r+1}}, \tag{10}$$

where the $r + 1$ plane lies below plane r.

What we now have is a simple algorithm for calculating the x-ray reflectivity of any multilayer structure which can be described as a set of discrete monolayers. The procedure is as follows.

(1) Calculate the substrate reflectivity R_0, using the standard Darwin theory.

(2) Calculate R_{-1} from Eq. (10), using input data q_{-1}, $q_{o,-1}$, and ϕ_{-1} corresponding to the composition and height of the first overlayer.

(3) Repeat for $R_{-2}, R_{-3}, \ldots$, up to R_{-N}, where N is the number of monolayers on top of the substrate.

(Note that this algorithm can calculate the x-ray reflectivity of a free-standing multilayer, i.e., unsupported by a bulk substrate, by simply setting $R_0 = 0$.)

This final reflectivity R_{-N} is valid for all angles above a few milliradians, including the strongly dynamical regions at the substrate Bragg peaks. There are no limitations on how abruptly the chemical composition can vary with depth. The results are exact for any planar structure of arbitrary composition profile, and with modern computers are simple to calculate.

III. APPLICATIONS OF THE DARWIN METHOD

The above Darwin algorithm for calculating x-ray reflectivities has been used to model the results of two sets of measurements, the first on a clean (004) surface of germanium, and the second an $Al_{0.3}Ga_{0.7}As/GaAs$ heterostructure. As a third application, calculations of the local electric field distribution in an overlayer with a linearly increasing lattice constant were carried out, where the reflectivity modulations are explained in simple physical terms using the moiré effect.

Experimental reflectivities were determined from triple-crystal diffractometry measurements,[16,17] where $K\alpha$ radiation from a sealed Cu-anode x-ray tube was first diffracted from a Ge(004) monochromator crystal, then by a specimen, and finally by a Ge(004) analyzer crystal, with the three crystals arranged in a nondispersive scattering geometry. The monochromator and the specimen were held in an ultrahigh vacuum (UHV) chamber equipped with Be x-ray windows. The source and monochromator were stationary, while θ, the angle of incidence onto the specimen, could be varied with a precision UHV rotation device. The specimen was rotated in a series of discrete steps through a substrate Bragg reflection, and at each step a scan of the analyzer crystal was taken. The analyzer scan measures the angular distribution of all of the x rays scattered by the specimen for a given value of θ; the area under this analyzer scan corresponds to the integrated intensity. Peak intensities exceeded 10^6 counts per second, and the background level far from the Bragg peak was below 2–3 counts per second, which for suitable counting times permitted a dynamic range of about seven orders of magnitude.[18]

A. Polished Ge (004) surface reflectivity

As the simplest possible extension of the ideal Darwin theory, we chose to examine a clean Ge(004) crystal maintained in ultrahigh vacuum. One might expect that the outermost layer of atoms at a crystal surface will reconstruct, which would modify the reflectivity of this layer. The first surface studied had been prepared by a standard sequence of mechanical grinding and polishing, a CP-4 chemical etch (acetic, nitric, and hydrofluoric acids at 1:2:1, plus bromine), finer regrinding, and finally Syton chemical polishing to produce an optically smooth finish. X-ray rocking curve scans showed the expected widths for a perfect crystal, demonstrating the absence of any gross strains or imperfections on the scale of the extinction depth. The reflectivity determined by triple-crystal diffractometry is shown in Fig. 2. In addition to the data points, the solid line shows the Darwin results for a perfect crystal, and the dashed line a best fit incorporating a near-surface strain, calculated with Eqs. (6) and (10), respectively.

It is clear that this specimen does not diffract as a perfect crystal away from the Bragg peak region. Several attempts to remount the specimen to eliminate any strain from the sample holder had no effect on the data. To further improve the surface condition, the crystal went through several cycles of Ar^+ ion sputtering and 630 °C anneals, again with no change in the deviation from the perfect crystal reflectivity. Examination of the surface with *in situ* reflection high-energy electron diffraction (RHEED) at first showed diffraction spots indicative of a "rough" surface. Roughness is a fitting parameter in several versions of kinematical surface diffraction, and we used the model described by Robinson.[19] A major limitation of all such kinematic models, however, is that the

dynamical Bragg peak data cannot be included. With the Bragg peak excluded, the best fit to the kinematic roughness model occurred for a root-mean-square roughness value of 45 Å, much larger than expected.

Not trusting this result, the specimen was further sputtered and annealed until the RHEED pattern showed streaks indicative of improved smoothness. Again the reflectivity data were unchanged. Armed with this independent verification of the surface smoothness from RHEED, it was clear that the kinematic surface roughness model was wrong. Finally, the specimen was removed from the chamber, re-etched in CP-4 to remove all possible strained material, and replaced in the chamber without further polishing. Now the measured reflectivity agreed quite well with the perfect crystal curve, indicating that the Syton-polished surface had residual near-surface strains. The dashed line through the original Syton-polished surface data in Fig. 2 is a fit using the Darwin algorithm, which models a compressive strain distributed over the top 50 atomic layers of the crystal. While the fit is fairly good, indicating the approximate validity of this strain model, the true microscopic structure is likely more complicated and would require additional data to determine.

These results demonstrate that an optically smooth, Syton-polished Ge specimen may still have significant strains which greatly perturb the reflectivity. This is important when using reflectivity to determine the structure of other epitaxial overlayers, since it is ordinarily assumed that a substrate with good rocking curves and RHEED patterns diffracts as a perfect crystal. We also show that the kinetic models' inability to include the peak reflectivity data can lead to incorrect conclusions. The Darwin approach models the reflectivity data over the entire range, from the dynamically diffracting Bragg peaks to the weakly scattering tails, and therefore provides a more stringent test of any structural model.

B. An $Al_{0.3}Ga_{0.7}As/GaAs$ heterostructure

The Darwin reflectivity calculation was also applied to triple-crystal diffractometry data from an $Al_{0.3}Ga_{0.7}As/GaAs$ heterostructure. Fabricated by standard MBE growth techniques, the specimen consisted of a 1000 Å layer of $Al_{0.3}Ga_{0.7}As$ which had been deposited onto a 1.1 μm GaAs buffer layer grown onto the GaAs substrate, topped by a final 50 Å layer of GaAs to protect the alloy layer from exposure to air. For the limited angular region about the [004] Bragg peak covered by the diffraction data, the specimen could be treated as just the 1000 Å alloy layer on an infinite GaAs substrate.

Figure 3 shows the reflectivity data and two curves generated by the Darwin reflectivity model. The dashed-line curve was the initial attempt to fit the data assuming an ideal structure: the composition changed abruptly from GaAs to $Al_{0.3}Ga_{0.7}As$ at the interface, and the two different lattice parameters were constant in their respective regions. The general trend of the data is reproduced, at least insofar as the thickness fringes, but the model is too simplistic.

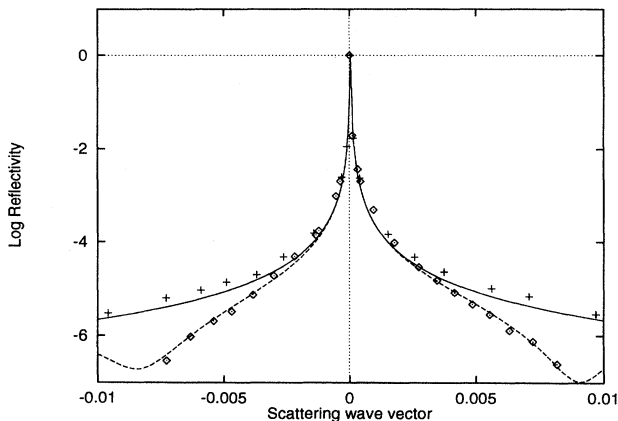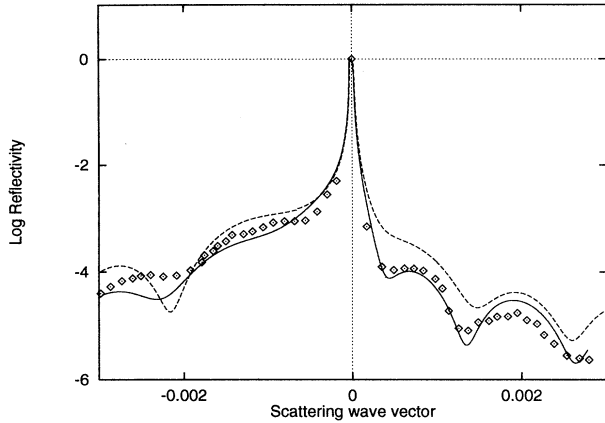To improve the fit, we modeled two physically expected

FIG. 2. [004] reflectivity of germanium, plotted versus the change in scattering wave vector in units of the [004] reciprocal lattice vector. The diamonds are initial triple-crystal reflectivity data for a clean, well-ordered surface, but the solid line is the theoretical reflectivity of a perfect crystal. The dashed-line fit to the data can be obtained by including excessive roughness, or by a slight near-surface compression (see text). After further chemical etching, the data (+) agree with the perfect crystal reflectivity.

FIG. 3. Logarithm (base 10) of [004] reflectivity of an MBE-grown $Al_{0.3}Ga_{0.7}As/GaAs$ heterostructure, plotted against the change in scattering wave vector, measured in units of the [004] reciprocal lattice vector. Two different fits are made to the data (diamonds). The dashed line assumes unperturbed lattice constants, while the solid line results from allowing the lattice parameters to vary linearly throughout the alloy layer.

phenomena: a gradual composition variation at the interface, due to interdiffusion and other surface effects during crystal growth, and a gradual variation in the lattice constant on both sides of the interface. The solid line in Fig. 3 shows the improved fit. It was at first surprising to find that an intermixing distance of nearly 70 Å was required when allowing the Al concentration to rise linearly from zero to its maximum value. This distance, corresponding to about 12 unit cells, is far greater than thermodynamic diffusion constants would predict. Consultations with the crystal grower revealed, however, that this is approximately the thickness of material grown while the Ga source ovens are cooling to reduce the flux of Ga by 30%. At the same time the Al source shutter is open, so there should be a region of gradually decreasing Ga concentration, consistent with the x-ray results.

The lattice parameter variation was modeled by a linearly increasing interplanar spacing which begins several hundred angstroms below the interface, in the pure GaAs substrate. Denoting the difference in the equilibrium GaAs and $Al_{0.3}Ga_{0.7}As$ lattice constants by δ, the lattice parameter in the 1000 Å alloy layer increased from the GaAs value, a_{GaAs}, to approximately $a_{GaAs} + 2\delta$. More sophisticated lattice parameter variations could produce better fits, but additional data would be required to justify these models. These results are sufficient to show that the lattice constants are perturbed over significant distances from the interface. Similar structural determinations of semiconductor heterostructures are routinely accomplished using algorithms based on the Takagi-Taupin theory; we demonstrate here that the conceptually simpler Darwin approach performs just as well. What we find especially appealing is that the calculation is done in exactly the same manner that the crystal grower uses in the MBE fabrication process: the

composition of the heterostructure is programmed one atomic layer at a time.

C. The effect of a linearly increasing lattice parameter

In traditional analyses of diffraction data, a set of distinct peaks is expected to correspond to a set of distinct lattice constants in the specimen. It has long been known, however, that a crystal whose lattice constant varies linearly with distance from the surface produces multiple reflectivity peaks not associated with distinct lattice constants.[15,18,19] That is, a MBE heterostructure which shows a Bragg peak split into two or more peaks may correspond to a linear strain, instead of two or more regions with distinct lattice constants. This curious situation has been modeled with both the Takagi-Taupin[17,20] and the Abelès theories,[4] and the nature of the modulation is understood on at least a mathematical basis. We apply the Darwin theory to this situation as an example of how the internal wave fields can be used to illustrate a simple, physical model for the modulated reflectivity.

In real specimens, linearly graded lattice parameters can be produced by appropriate doping, such as with boron-doped epitaxial layers of silicon on a silicon substrate,[20,21] α particle radiation damage,[22] or as a consequence of accommodating a lattice mismatch, as in the previous example. To focus attention on the role of the lattice parameter alone, we consider a hypothetical structure consisting of a (001) perfect Ge substrate with 20 000 atomic planes of Ge whose successive interplanar spacing is given by

$$d_m = (1 + m\delta)d_0. \tag{11}$$

Here d_0 is the bulk interplanar spacing, i.e., the [004] lattice constant, m is the index of the plane which runs from $m = 1$ at the substrate interface to $m = 20\,000$ at the surface, and δ is the lattice parameter expansion factor which was set to 5×10^{-8}. All calculations were done for an x-ray energy of 8 keV. Figure 4(a) displays the reflectivity in the neighborhood of the [004] Bragg peak, revealing nine peaks on the low-angle side of the (diminished) Darwin peak. (Computing the 20 000 recursions at each incident angle required less than 2 s CPU time on a 12 "Megaflop" computer.)

An understanding of this effect comes from considering the fields within the overlayer region. For all angles θ in the low-angle, modulated part of the reflectivity spectrum, the incident beam satisfies the Bragg condition, $n\lambda = 2d_m \sin\theta$, for some plane m within the overlayer. For such a small expansion factor, $\delta = 5 \times 10^{-8}$, there will be a large number of nearby planes for which the Bragg condition is almost met, which will generate a diffracted beam of significant amplitude. All of the planes between the diffracting depth and the surface will therefore be interacting with the standing wave field created by the interference between the incident and diffracted beams. The standing wave field will have the periodicity of the diffracting planes, d_m, but the lattice spacing is linearly increasing, causing successive planes to gradually move in
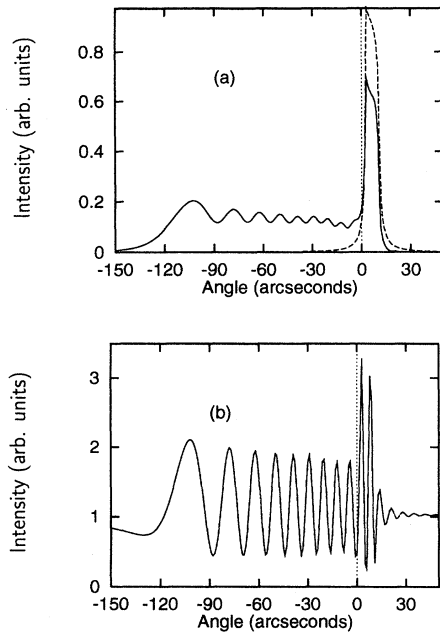
FIG. 4. (a) [004] Ge reflectivity with linearly increasing layer spacing. The solid curve is the calculated reflectivity for a crystal with 20 000 atomic planes of Ge on top of a perfect Ge substrate, in which the interlayer spacing increases linearly from the interface up to the surface. The fractional increase per layer is 5×10^{-8}. Curves are plotted against the angle of incidence with respect to the [004] nominal Bragg angle. The dashed line is the Darwin reflectivity for a perfect crystal. (b) The net intensity at the topmost layer as a function of the angle of incidence.
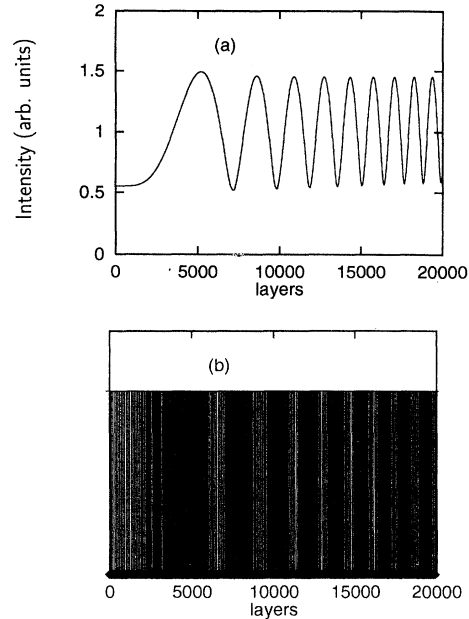

FIG. 5. (a) The net intensity as a function of layer number, at the nominal Bragg angle of incidence. The pattern is consistent with a standing wave of fixed period d_m being generated near the first peak at $m = 5000$, which goes in and out of phase with the linearly expanding lattice above. (b) A moiré pattern obtained by overlaying a set of lines with constant spacing with another set of lines having a linearly increasing spacing. The expansion factor matches that of the hypothetical Ge specimen in part (a). Note the similarity of (a) and (b).

and out of phase with the standing wave field. For example, the diffracting region is in the near-surface region for the first maximum seen at $\theta = -102$ arc sec. The intensity decreases to a minimum around -88 arc sec because the diffracting region has moved deeper into the crystal, causing the near-surface region to be out of phase with the standing wave field and thereby leading to a decrease in the net scattered beam. The intensity increases again with increasing θ as the near-surface region is again in phase with the standing wave.

The modulation of the wave field intensity at the surface is obtained from the product $a(m)a(m)^*$, where $a(m)$ is the total amplitude $t(m) + s(m)$ evaluated at the surface (e.g., $m = 20\,000$). This is shown in Fig. 4(b), where it is immediately seen that the modulation of the reflectivity on the low-angle side of the Bragg peak is exactly mirrored by the the standing wave intensity at the surface. As the origin of the diffracted wave moves deeper into the crystal, the total reflectivity increases whenever the surface is back in phase with standing wave. This can be seen even more clearly by selecting a definite angle of incidence and calculating the wave field intensity as a function of depth into the crystal. Figure 5(a) illustrates the modulation of the internal intensity for the angle of incidence at the nominal bulk Bragg angle (i.e., at the 0.0 arc sec position of Fig. 4). Once again, the modula-

tions in the reflectivity [Fig. 4(a)] are exactly mirrored by the internal intensity distribution. This confirms the physical picture that the standing wave which originates at a given depth for a given angle of incidence determines the overall diffracted intensity, depending on the relative fraction of atomic planes above that depth which are either in phase or out of phase with the wave field.

This physical model is further illustrated in Fig. 5(b), a moiré pattern which is the sum of two line patterns, the first representing the constant spacing of the standing wave field, and the second having the linearly increasing separation given by the value of $\delta = 5 \times 10^{-8}$. The two patterns are in alignment at the interface ($m = 0$), and the ensuing nine regions of low and high line density agree nicely with the interior intensity modulation in Fig. 5(a). Note that the first high-density region near $m = 5000$ layers, corresponding to the two lattices being out of phase, should be matched with the first minimum in the wave field intensity near $m = 7000$ layers. This offset is merely the "index of refraction" correction, which shifts the actual Bragg condition at the interface ($m = 0$) to an incident angle several arc sec above the nominal Bragg angle.

The curves in Figs. 4(b) and 5(a) illustrate the insight available from consideration of the internal wave field distribution on the atomic planes, a feature which is the es-

sential characteristic of the Darwin method. This could be easily extended to calculating the secondary yield due to the interactions with the wave field, i.e., the standing wave yield from an arbitrary heterostructure.[23-25] For each plane in the structure, secondary production (of fluorescence, photoelectrons, Auger electons, etc.) is generally proportional to the local intensity, and the yield then depends only on the probability of escape from the specimen. Standing wave yields can be calculated in this manner from planar heterostructures of arbitrary complexity.

IV. CONCLUSIONS

The x-ray reflectivity of any structure made up of parallel atomic planes can be calculated using the Darwin recursion relations. The results are valid for any composition profile, and are equally exact at intense Bragg peaks and in the weak tails of a reflection. This method has been applied here to problems involving near-surface perturbations in a bulk Ge crystal, an $Al_{0.3}Ga_{0.7}As/GaAs$ MBE-grown heterostructure, and a theoretical investigation of a perfect crystal with a linearly increasing lattice parameter. The Darwin method explicitly determines the wave fields at each of the atomic planes in the structure, and therefore provides a picture of the wave field distribution inside the structure which can be used for standing wave studies, for example. While this method has much in common with other approaches, e.g., the Takagi-Taupin equations and the Abelès matrix approach, it is uniquely built upon the reflectivity of the individual atomic planes. Using the Darwin theory of heterostructure diffraction, both the design of MBE-grown heterostructures and the calculation of the heterostructure reflectivity have the same focus: the order and composition of individual atomic planes.

ACKNOWLEDGMENTS

[1] S. Takagi, Acta Crystallogr. **15**, 1131 (1962); J. Phys. Soc. Jpn. **26**, 1239 (1969).

[2] D. Taupin, Bull. Soc. Fr. Mineral. Cristallogr. **87**, 469 (1964).

[3] D. W. Berreman, Phys. Rev. B **14**, 4313 (1976); **19**, 560 (1979); D. W. Berreman and A. T. Macrander, ibid. **37**, 6030 (1988).

[4] A. T. Macrander, E. R. Minami, and D. W. Berreman, J. Appl. Phys. **60**, 1364 (1986).

[5] M. Born and E. Wolf, Principles of Optics, 6th ed. (Pergamon Press, Oxford, 1993).

[6] M. von Laue, Ergeb. Exakten. Naturwiss. **10**, 133 (1931).

[7] W. J. Bartels, J. Hornstra, and D. J. W. Lobeek, Acta Crystallogr. Sec. A **42**, 539 (1986).

[8] S. P. Darbinyan, P. V. Petrashen', and F. N. Chukhovskii, Pis'ma Zh. Eksp. Teor. Fiz. **55**, 618 (1992) [JETP Lett. **55**, 642 (1992)].

[9] L. G. Parratt, Phys. Rev. **95**, 359 (1954).

[10] L. L. Chang, Armin Segmüller, and L. Esaki, Appl. Phys. Lett. **28**, 39 (1976).

[11] C. G. Darwin, Philos. Mag. **27**, 315 (1914); **27**, 675 (1914).

[12] A. Howie and M. J. Whelan, Proc. R. Soc. London Ser. A **263**, 217 (1961); see also B. S. Borie, Acta Crystallogr. **21**, 470 (1966).

[13] Z. Pinsker, Dynamical Scattering of X-Rays in Crystals (Springer-Verlag, Berlin, 1978), p. 371.

[14] S. Nakatani and T. Takahashi, Sur. Sci. **331**, 433 (1994).

[15] S. Durbin, Acta Crystallogr. (to be published).

[16] P. Eisenberger, N. G. Alexandropoulos, and P. M. Platzman, Phys. Rev. Lett. **28**, 1519 (1972).

[17] A. M. Afanas'ev, M. V. Kovalchuk, E. K. Kovev, and V. G. Kohn, Phys. Status Solidi A **42**, 415 (1977).

[18] G. C. Follis, Ph.D. thesis, Purdue University, 1993.

[19] I. K. Robinson, in Handbook on Synchrotron Radiation, edited by G. Brown and D. Moncton (Elsevier, New York, 1991), Vol. 3, Chap. 7.

[20] Akira Fukuhara and Yukio Takano, Acta Crystallogr. Sec. A **33**, 137 (1977).

[21] Akira Fukuhara and Yukio Takano, J. Appl. Crystallogr. **13**, 391 (1980).

[22] J. Burgeat and R. Colella, J. Appl. Phys. **40**, 3505 (1969).

[23] B. W. Batterman, Phys. Rev. **133**, A749 (1964); Phys. Rev. Lett. **22**, 703 (1969).

[24] J. A. Golovchenko, B. W. Batterman, and W. L. Brown, Phys. Rev. B **10**, 429 (1974).

[25] S. M. Durbin, L. E. Berman, B. W. Batterman, and J. E. Blakely, Phys. Rev. B **33**, 4402 (1986).